Molecular dynamics determination of the surface tension of silver–gold liquid alloys and the Tolman length of nanoalloys

ARTICLE *in* THE JOURNAL OF CHEMICAL PHYSICS · APRIL 2012

Impact Factor: 2.95 · DOI: 10.1063/1.3701372 · Source: PubMed

1 AUTHOR:

Florent Calvo
University Joseph Fourier - Grenoble 1
211 PUBLICATIONS **3,549** CITATIONS

Molecular dynamics determination of the surface tension of silver-gold liquid alloys and the Tolman length of nanoalloys

F. Calvo

Citation: J. Chem. Phys. **136**, 154701 (2012); doi: 10.1063/1.3701372
View online: http://dx.doi.org/10.1063/1.3701372
View Table of Contents: http://jcp.aip.org/resource/1/JCPSA6/v136/i15
Published by the American Institute of Physics.

Molecular dynamics determination of the surface tension of silver-gold liquid alloys and the Tolman length of nanoalloys

F. Calvo[a)]
LASIM, Université de Lyon and CNRS UMR 5579, 43 Bd du 11 Novembre 1918, F69622 Villeurbanne Cedex, France

(Received 13 February 2012; accepted 20 March 2012; published online 16 April 2012)

Using molecular dynamics simulations, an embedded-atom model potential, and the mechanistic route, we have computed the pressure tensor and the surface tension γ of Ag-Au liquid alloys. Although the model generally underestimates γ for pure metals, calculations for a bulk planar slab exhibit nonlinear variations of γ with increasing gold concentration, which agree with experiments and can be accounted for by a perfect solution model. Calculations for various nanoscale droplets containing between 100 and 3200 atoms show a systematic decrease of γ with increasing droplet radius R. The positive Tolman length of the alloy determined from these size variations is estimated to vary slightly with gold concentration. The effects of temperature in the range 1300–1700 K are discussed. © *2012 American Institute of Physics*. [http://dx.doi.org/10.1063/1.3701372]

I. INTRODUCTION

Surface tension is a key thermodynamical parameter of free surfaces and interfaces, which expresses that surface atoms or molecules are not as tightly bound as those in the bulk volume. It is an important quantity in fundamental problems such as nucleation or cavitation models, but it is also strongly involved in technological applications ranging from sprays and aerosols to crystal growth or welding.

In the case of liquid metals, measurements of the surface tension γ are difficult, owing to the high reactivity with the environment (oxygen especially) that occurs at the necessary high temperatures.[1] Heterogeneous systems are particularly interesting, because impurities with lower surface tension are expected to move to the surface in order to minimize the global free energy. However, this picture is complicated by other factors that affect ordering and segregation, such as atomic size ratio or mixing energies. In this respect, metal alloys offer convenient systems to unravel the complex interplay between atomistic properties and macroscopic observables.

Most theoretical efforts devoted to understanding the surface tension of mixed systems have relied on semi-empirical thermodynamical modeling, in which experimental data are used as input. Many such models are rooted in the so-called Butler equation,[2] which considers the surface as a separate monolayer interface between the bulk liquid and the vapor phase. Alternatively, molecular simulation can give a lot of physical insight into the surface properties of liquid metals and alloys alike. The numerical approach combines some atomistic description of the interatomic forces with a dedicated computational protocol to extract γ. For noble and transition metals, reasonably accurate many-body potentials can be found in the embedded-atom model (EAM) family.[3] Two main strategies are available to determine numerically the surface tension of bulk liquids, based either on purely thermodynamical considerations or on the momentum transfer across the interface at mechanical equilibrium.

Such numerical experiments have been employed quite often in the past to evaluate the surface tension of planar slabs of pure liquids[4–8] and, only occasionally, of liquid mixtures.[9–11] Computer simulations are particularly useful for addressing liquid droplets at the nanoscale. Interfacial effects become dominant in small droplets, simply because of the magnitude reached by the surface/volume ratio. The variations of the surface tension at small size were first recognized by Tolman,[13] who in his pioneering thermodynamical theory found that γ for a spherical droplet of radius R should vary as

$$\gamma(R) = \gamma(\infty)\frac{R}{R+2\delta} \simeq \gamma(\infty)\left(1-2\frac{\delta}{R}\right), \qquad (1)$$

$\gamma(\infty)$ denoting the surface tension in the bulk limit of vanishing curvature. The parameter δ, known as the Tolman length, is expected to be of typical interatomic length. The above equation looks similar to liquid drop expansions in inverse powers of R, the correcting term varying as $1/R^2$. However, the Tolman length is essentially unknown for most natural compounds, and our current knowledge of this quantity originates from various computations. Simulations[15,16] and density-functional theory[17–20] calculations carried out for Lennard-Jones (LJ) fluids have led to somewhat controversial conclusions[11,12,14] about the sign of δ, before growing evidence suggested that the Tolman length may indeed be very small in such weakly bound systems.[11,12]

However, for metals the available data are scarce. Thermodynamical approaches indicate that δ should be positive for mercury.[14] Recent experimental measurements on gallium,[21] as quoted by Masada and Sawada[22] who supported these results by molecular dynamics simulations, confirm that the surface tension of liquid metal droplets decreases at small sizes, but the Tolman length seemed difficult to evaluate from these simulations.

a)Electronic mail: fcalvo@lasim.univ-lyon1.fr.

In the present work, we aim to examine the situation in liquid silver-gold, both in the bulk and nanoscale phases. In the condensed matter limit, these two elements readily mix with the alloy having a simple phase diagram.[23] Bulk surfaces[24] experimentally show a moderate enrichment in silver, and the same behavior has been observed in nanoparticles[25,26] and confirmed by theory.[27,28] Following previous efforts from other groups, we use molecular simulation to compute the surface tension of the alloy in bulk slabs and finite droplets. Our results indicate a minor but visible surface enrichment in silver, and a nonlinear dependence of the surface tension with increasing gold concentration. The surface tension obtained for liquid droplets clearly shows some depression relative to the bulk slab, and an approximate Tolman length can be inferred from the variations of γ with $1/R$. The Tolman length is found to increase slightly with temperature and gold concentration as well.

Turning to the main body of the paper, we briefly describe in Sec. II the computational methods used to model the interactions, as well as the strategy to determine the surface tension of the bulk and finite droplets in the liquid state. Section III presents and discusses our results, and some concluding remarks are finally given in Sec. IV.

II. METHODS

There are mainly two numerical strategies to compute surface tensions from molecular simulations, known as the mechanical and thermodynamical routes, respectively.[29] The latter method consists of evaluating the surface tension from the work of cohesion associated to the formation of the interface. It only requires statistical averages of energetic properties, and is thus general and relatively straightforward to apply in systems with arbitrarily complex potentials, especially by Monte Carlo integration. On the other hand, the former method relies on the calculation of the surface stress tensor, which involves the forces on the individual particles, and is thus naturally convenient in the framework of molecular dynamics. The equivalence between the mechanical and thermodynamical methods was originally proven by Buff in the case of pair potentials,[29] and generalized more recently by Masada and Sawada.[22] In the present work, the mechanical method has been followed.

A. Potential

Metallic binding in bulk and nanoscale Ag-Au alloys is modeled using the many-body potential obtained from the second moment approximation (SMA) to the electronic density of states in tight-binding theory. The potential V for a general configuration $\mathbf{R}$ of the N atoms is expressed as a sum of a pairwise repulsive contribution that accounts for short-range Pauli repulsion, and an additive, many-body cohesive contribution that is a simple function of a local electronic density ρ,

$$V(\mathbf{R}) = \frac{1}{2}\sum_{i,j}\varepsilon_{ij}\exp\left[-p_{ij}\left(\frac{r_{ij}}{r_{ij}^{(0)}}-1\right)\right] - \sum_i \sqrt{\rho_i}, \tag{2}$$

where r_{ij} denotes the distance between atoms i and j, and ρ_i is expressed as

$$\rho_i = \sum_{j\neq i}\zeta_{ij}^2\exp\left[-2q_{ij}\left(\frac{r_{ij}}{r_{ij}^{(0)}}-1\right)\right]. \tag{3}$$

The 15 parameters of the model, namely ε_{ij}, ζ_{ij}, p_{ij}, q_{ij}, and $r_{ij}^{(0)}$, were taken from Rapallo *et al.*,[30] who refined the original set of Cleri and Rosato.[31] The SMA potential predicts a surface enrichment in silver in nanoclusters at low temperature,[28] but an order/disorder transition takes place as well.[32] This potential was recently used to address the vibrational properties of Ag-Au nanoalloys.[33]

B. Pressure tensor and surface tension

We first consider a planar interface separating a condensed phase from the vapor phase. The pressure tensor has two components p_{N} and p_{T}, respectively, normal and tangential to the interface, which we assume to be parallel to the z Cartesian coordinate. p_{T} is obtained from the statistical average of the xx and yy components of the stress tensor $\boldsymbol{\sigma}$ as

$$\begin{aligned} p_{\mathrm{T}} &= -\langle\sigma^{xx}\rangle - \langle\sigma^{yy}\rangle \\ &= \frac{1}{S}\left\langle\sum_i \frac{\left(p_i^x\right)^2+\left(p_i^y\right)^2}{m_i} + \sum_{i\neq j} x_{ij}f_{ij}^x + y_{ij}f_{ij}^y\right\rangle, \end{aligned} \tag{4}$$

where S is the area of the interface, p_i^x is the x component of the momentum of atom i with mass m_i, $x_{ij}=x_j-x_i$, and f_{ij}^x the x component of the force exerted by i on j. Similarly p_{N} reads

$$p_{\mathrm{N}} = -\langle\sigma^{zz}\rangle = \frac{1}{S}\left\langle\sum_i\frac{\left(p_i^z\right)^2}{m_i} + \sum_{i\neq j} z_{ij}f_{ij}^z\right\rangle. \tag{5}$$

It should be emphasized here that in the above expressions, although the contributions of the forces to the pressure appear as in a pairwise form, all terms f_{ij} may be complex functions of atomic coordinates.[34] In the case of the many-body SMA potential of Eq. (2), the x component is written as

$$\begin{aligned} f_{ij}^x = {} & p_{ij}\varepsilon_{ij}\frac{x_{ij}}{r_{ij}r_{ij}^{(0)}}\exp\left[-p_{ij}\left(\frac{r_{ij}}{r_{ij}^{(0)}}-1\right)\right] \\ & - x_{ij}q_{ij}\frac{\rho_i^{-1/2}+\rho_j^{-1/2}}{r_{ij}r_{ij}^{(0)}}\zeta_{ij}^2\exp\left[-2q_{ij}\left(\frac{r_{ij}}{r_{ij}^{(0)}}-1\right)\right]. \end{aligned} \tag{6}$$

The surface tension γ is obtained from the integrated difference between the normal and tangential components of the pressure tensor[29]

$$\gamma = \int_0^\infty [p_{\mathrm{N}}(z)-p_{\mathrm{T}}(z)]dz. \tag{7}$$

Unfortunately, curved surfaces are more difficult to treat, because of the non-uniqueness of the pressure tensor in other coordinate systems. In the case of spherical droplets, the surface tension γ can still be expressed from the pressure

difference as[29]

$$\gamma = \int_0^\infty \left(\frac{r}{R}\right)^2 [p_N(r) - p_T(r)]dr, \quad (8)$$

where R is the droplet radius. Both the tangential and normal components of the pressure tensor are no longer explicit, but analytical forms exist in which the contributions involving atoms i and j are continuously integrated over the line separating them.[35] Following Masada and Sawada,[22] we use the approach by Ikeshoji and co-workers[36] to evaluate the components p_N and p_T from the line integrals separating i from j.

C. Computational details

Molecular dynamics were carried out at constant temperature in the range 1300–1700 K using the Nosé-Hoover method, with a time step of 5 fs. The surface tension of bulk liquid was obtained by simulating a liquid slab, starting from a face-centered cubic sample of 2048 atoms at experimental density. Periodic boundary conditions in the minimum image convention were implemented in all three directions, with a box length in the z direction (normal to the interface) twice as large as the x and y length.

Droplets containing 100, 200, 400, 800, 1600, and 3200 atoms were simulated, starting from incomplete icosahedral structures and using periodic boundary conditions with a cubic box length equal to approximately twice the droplet radius.

For all systems, the gold concentration c_{Au} was varied from 0 to 1 by steps of 10%, gold and silver atoms being randomized within the initial lattice structure. For the bulk slabs, each simulation was propagated for 1.5 ns, with statistical averages being accumulated over the last nanosecond. For the droplets, and in order of increasing size, the simulations were propagated for 10, 10, 5, 3, 2, and 1 ns, respectively, after some preliminary 50% of equilibration time. The simulations were repeated 10 independent times, with a measurable dispersion contributing to the error bars.

III. RESULTS AND DISCUSSION

The various MD simulations performed in this work are aimed at evaluating the respective roles of size, composition, and temperature on the surface properties of liquid Ag-Au alloys in bulk and nanoscale phases. Although our main goal is to calculate the surface tension, we have first investigated the structural behavior of the slab and the droplets.

A. Surface enrichment in bulk and nanoscale alloys

Based on thermodynamical arguments, silver-gold alloys were originally thought to exhibit some enrichment in silver at the surface due to the lower surface energy reported for this metal.[37] Even though the first Auger measurements contradicted this statement,[38] there seems now to be general consensus about the existence of a slight enrichment in silver in bulk alloys, within about one monolayer only.[24,27] More recently, the same conclusions were reached for silver-gold nanoalloys.[25,26,28]

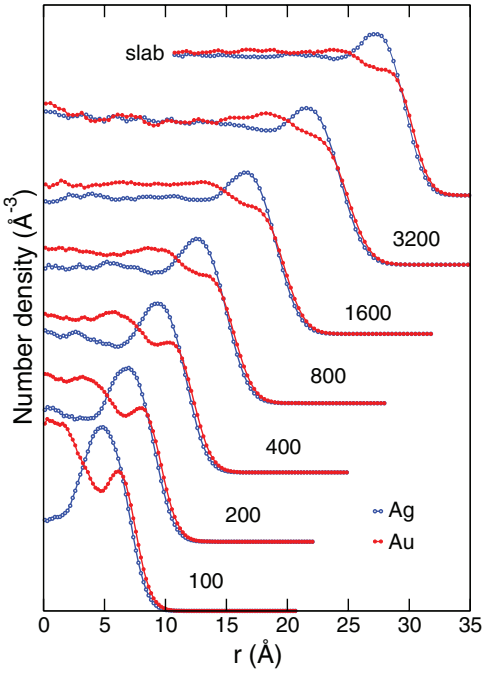

FIG. 1. Number densities of silver and gold atoms in a Ag-Au liquid slab and in liquid droplets with various sizes, at equiconcentration and $T = 1500$ K. For clarity, the curves have been shifted vertically and horizontally in the case of the slab.

We have represented in Fig. 1 the number densities of silver and gold atoms in their liquid alloy, at equiconcentration and $T = 1500$ K, in both the bulk slab and the liquid droplets.

In all systems, there is a small but visible higher relative amount of silver in the outer part. This enrichment occurs over a few Å, which is about the size of a monolayer. Inside the bulk liquid slab, the perfect solution is recovered below this layer.

However, in finite droplets containing up to 1600 atoms, the inner composition is comparatively enriched in gold. This is a pure compensation originating from the conservation of global mass. As the droplet size increases, the relative surface enrichment in silver decreases from 17% (for $N = 100$) to 12% (for $N = 200$), 9% (for $N = 400$) and eventually converges to 8% in the bulk limit.

The present results are consistent with current literature,[24,27] and with the computational results obtained by Rossi *et al.*[28] who used the same SMA potential, but in concern with low-temperature conformations rather than the high-temperature melted state. Since mixing is favorable for the Ag-Au alloy and the two elements have nearly the same atomic radii, there is thus strong evidence that the surface energy of silver is lower than that of gold with the present model.

B. Surface tension of bulk alloys

In the mechanical approach, the surface tension is obtained by integrating the difference between the normal and tangential components of the pressure tensor through the vapor-liquid interfaces. Since the liquid slab is symmetric around $z = 0$, the integration of Eq. (7) is performed between

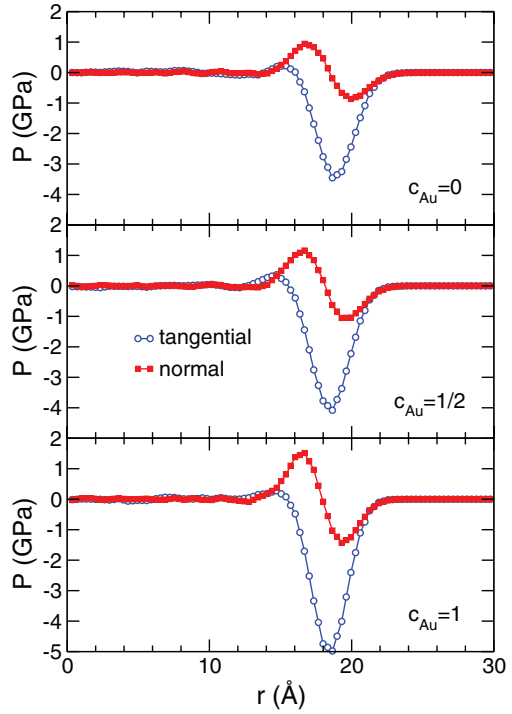

FIG. 2. Tangential and normal components of the pressure tensor across the liquid-vapor interface in Ag-Au liquid slabs at different gold concentrations c_{Au}, and $T = 1500$ K.

$z = -\infty$ and $z = +\infty$ but the result is divided by 2 to account for the two interfaces.

The profiles of the pressure components with varying distance to the center of the slab are represented in Fig. 2 for three typical gold concentrations, at $T = 1500$ K.

The net pressure is only nonzero around the interface, where the gradient of the potential experiences its most abrupt variations. As in previous work,[22] the tangential pressure exhibits strongly negative values concomitant to the drop in density, and the minimum of a few gigapascals increases with gold concentration.

The normal pressure reaches a positive maximum deeper in the liquid phase, but also a negative minimum in the outer parts of the droplet. This behavior contrasts with the results obtained for gallium slabs, where no significant variations were reported.[22] This difference could be due to the different potentials used for the two metals, but also to the much higher temperature considered by the authors of Ref. 22.

The surface tension resulting from the integration of $p_{\mathrm{N}} - p_{\mathrm{T}}$ across the slab was calculated for three temperatures in the range 1300–1700 K. The variations of γ with increasing gold concentration are reported in Fig. 3, where the error bars convey the statistical dispersion associated with the averages over 10 independent simulations.

The values obtained for the pure metals can be compared to experiment.[39] In both cases, the surface tension is underestimated significantly, by about 20%–30%. Such a discrepancy was also reported by previous authors using similar but differently parametrized many-body potentials.[6,8] It is likely ascribable to the relative crudeness of the present EAM potential, and the agreement with experiment should improve

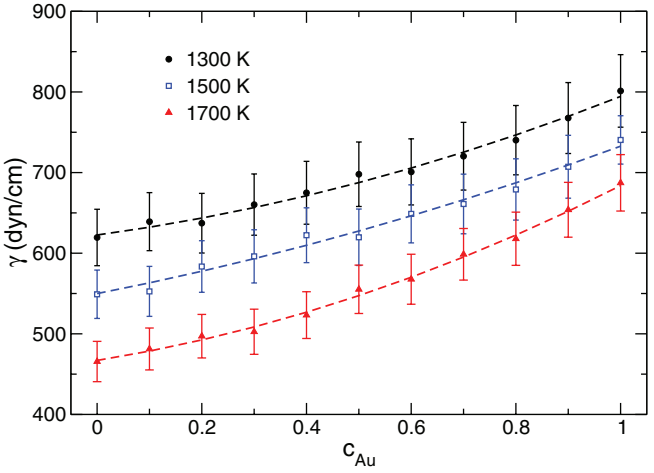

FIG. 3. Surface tension in Ag-Au liquid slabs, for different gold concentrations c_{Au}, at 1300, 1500, and 1700 K. The dashed lines are the predictions of the perfect solution model, Eq. (9), after optimizing the atomic area A.

by considering gradient corrections in the local density, following here Webb and Grest.[6]

The variations of the surface tension γ with increasing gold concentration c_{Au} are clearly nonlinear, in agreement with experimental measurements by Bernard and Lupis.[40] The convexity of these variations suggests that silver contributes more than gold to the global value of γ, which according to Yu and Stroud[10] would be consistent with the surface enrichment in silver found in Sec. III A. However, it can also be explained using the simple thermodynamical argument of a perfect solution, in which the free energy at the interface is written as the composition-averaged value of the pure elements:[40]

$$\exp\left[-\frac{\gamma(c_{\mathrm{Au}})A}{k_{\mathrm{B}}T}\right] = (1-c_{\mathrm{Au}})\exp\left(-\frac{\gamma_{\mathrm{Ag}}A}{k_{\mathrm{B}}T}\right) + c_{\mathrm{Au}}\exp\left(-\frac{\gamma_{\mathrm{Au}}A}{k_{\mathrm{B}}T}\right). \quad (9)$$

In this equation, $\gamma_{\mathrm{Ag}} = \gamma(c_{\mathrm{Au}} = 0)$ and $\gamma_{\mathrm{Au}} = \gamma(c_{\mathrm{Au}} = 1)$ denote the surface tensions of pure silver and gold, respectively, and A is the common average atomic area of silver and gold. The perfect solution model provides a template for representing the variations of $\gamma(c_{\mathrm{Au}})$ by optimizing the value of A across the range $0 \le c_{\mathrm{Au}} \le 1$.

In practice, setting A close to 17 Å^2 gives a quantitative account of the variations of the surface tension across the entire concentration range, at the three temperatures considered. Although somewhat higher than the value experimentally reported by Bernard and Lupis,[40] this value is comparable to the natural atomic area $\pi[r^{(0)}]^2$ obtained from the atomic radii $r^{(0)}$ of gold and silver, which further supports the validity of the perfect solution model.

C. Surface tension of nanodroplets

Silver-gold liquid droplets simulated at the same temperature have been analyzed in terms of their density and stress tensor. The droplet radius R was obtained by fitting the overall

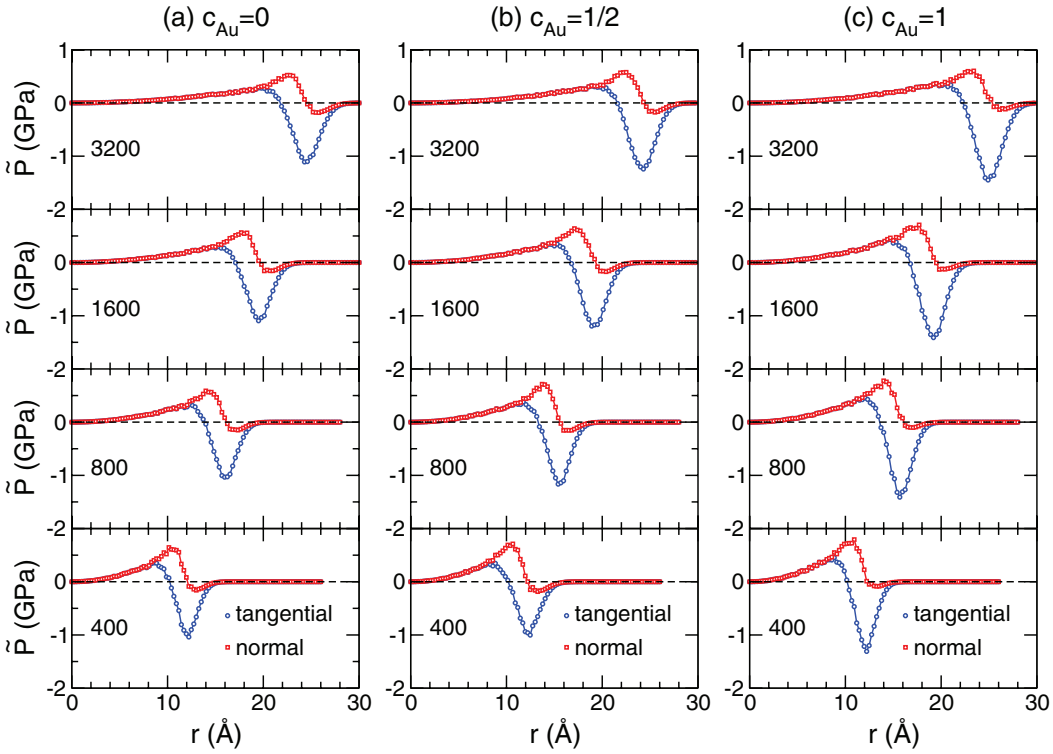

FIG. 4. Tangential and normal components of the scaled pressure tensor $\widetilde{P}(r) = (r/R)^2 P(r)$ across the liquid-vapor interface in Ag-Au liquid droplets for different sizes and for gold concentrations of (a) $c_{\mathrm{Au}} = 0$; (b) $c_{\mathrm{Au}} = 1/2$; and (c) $c_{\mathrm{Au}} = 1$. The temperature is 1500 K.

density profile to an hyperbolic tangent function.[41] The variations of the normal and tangential components of the pressure tensor with increasing radius are represented in Fig. 4 for various droplet sizes in the case of the pure metals and at equiconcentration, at $T = 1500$ K. For a better comparison with the liquid slab, we show the scaled pressure tensor $\widetilde{P}_{\mathrm{N}}(r) = (r/R)^2 P_{\mathrm{N}}(r)$ and $\widetilde{P}_{\mathrm{T}}(r) = (r/R)^2 P_{\mathrm{T}}(r)$, from which the surface tension is obtained by integration of the difference. The variations of the scaled pressure components with radial distance are rather similar to those of the pure components in the bulk slab, close to the vapor interface. However, near the center of the droplet the pressure is nonzero and, by virtue of the Laplace equation it even increases linearly with inverse radius. This behavior is reflected in the steady increase of both components of the scaled pressure tensor, although the difference between them remains minor. The tangential pressure drops at the liquid-vapor interface, and the minimum reached decreases with droplet size, although this effect is masked on the scaled variables. Conversely, the range where these variations are stronger does not significantly change with size. This behavior is similar to the number density (see Fig. 1) and indicates a direct connection between these two quantities. The scaled pressure varies by similar magnitude for all droplet sizes, thus the real (unscaled) pressure increases with radius. This already suggests that the surface tension will be lower for droplets than it is for the bulk slab. Assessing now the effect of the gold concentration, the pressures increase in magnitude as c_{Au} increases from 0 to 1.

The surface tension resulting from these pressure components is shown in Fig. 5 for the various droplet sizes, at $T = 1500$ K and for increasing gold concentration. As anticipated based on the pressure components, the surface tension of the liquid droplets are significantly lower than the bulk value, and this will be studied in more quantitative details below. Similarly to the bulk slab, mixing gold and silver yields a surface tension that is notably lower than the linear extrapolation between the pure metals. It is possible to model the variations of γ with c_{Au} according to the perfect solution model [Eq. (9)], provided that the effective atomic area A is adjusted. Such an adjustment gives a very satisfactory representation of the effects of alloying on the surface tension, at

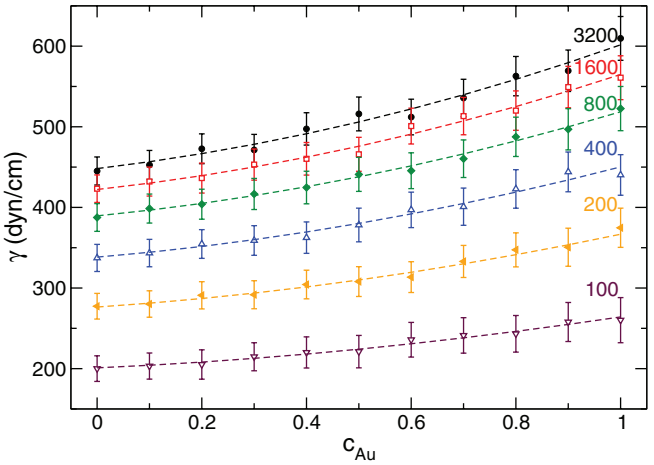

FIG. 5. Surface tension in Ag-Au liquid droplets with different sizes (indicated on the right), as a function of gold concentration c_{Au} and at $T = 1500$ K. The dashed lines are the predictions of the perfect solution model, Eq. (9), after optimizing the atomic area A.

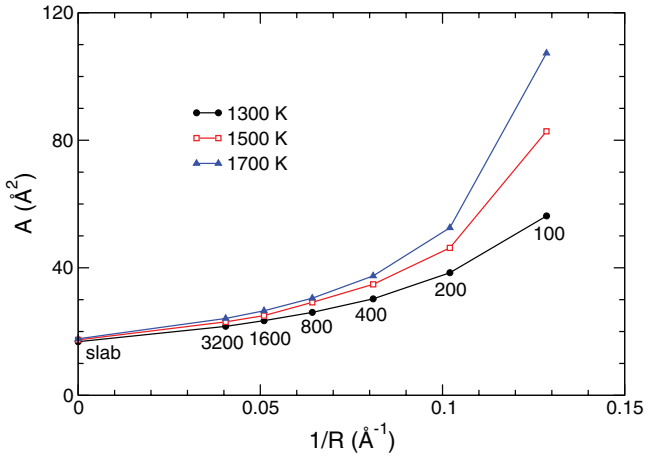

FIG. 6. Effective atomic area A of bulk and nanoscale Ag-Au liquid alloys in the perfect solution model, as a function of curvature. A was obtained by optimizing Eq. (9) over the composition range, at three different temperatures.

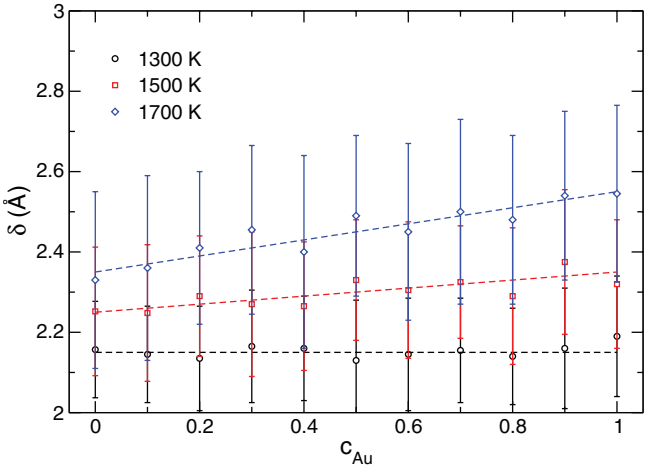

FIG. 8. Tolman length δ of Ag-Au liquid droplets inferred from the size variations of the surface tension, as a function of gold concentration c_{Au} and for the three temperatures $T = 1300$, 1500, and 1700 K. The dashed lines are the best linear fits.

least considering the extent of the error bars in the MD simulation.

It is interesting to consider the effective atomic area A and the respective roles of size and temperature. The variations of A with droplet curvature ($1/R$) are shown in Fig. 6, together with the value obtained for the bulk slab (at $1/R \to 0$). The atomic area strongly increases with curvature, and also with temperature, especially for the smallest droplets. Such increases are concomitant with the spreading of droplets at small sizes, the homogeneous, bulk-like liquid proportion being comparable or even marginal compared to the size of the interface.

D. Tolman length

The surface tensions of liquid droplets and the liquid slab, as obtained from the MD simulations, are represented in Fig. 7 against curvature, for the pure metals and at equiconcentration. γ strongly decreases with the inverse droplet radius, an effect also reported experimentally and theoretically in hot gallium droplets.[21,22]

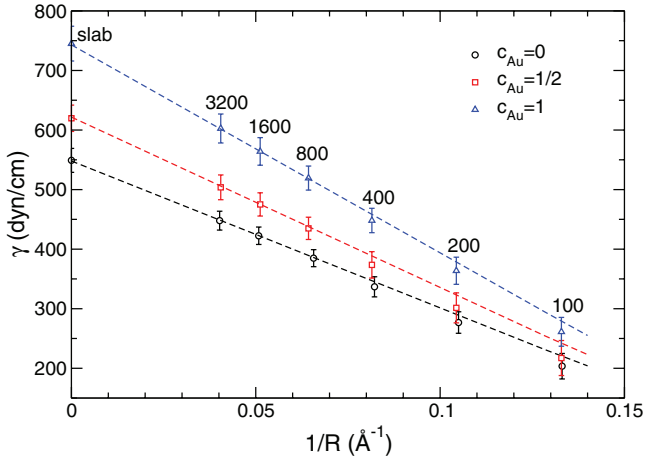

FIG. 7. Surface tension of Ag-Au liquid droplets as a function of inverse radius, for three gold concentrations and at $T = 1500$ K. The value at $1/R = 0$ corresponds to the liquid slab.

The variations of γ with $1/R$ follow approximately linear variations, at least in the largest droplets with $N > 400$ atoms, which is a clear signature of nonzero and positive Tolman length in the pure metals and in the alloys. However, the values for the smallest droplets lie away from the linear interpolation, which suggests that the higher order term in $1/R^2$ is not negligible (and also positive). This result agrees with previous theoretical analyses,[18] even though the threshold for the validity of the Tolman expansion differs here from the value of $N \sim 10^6$ atoms in LJ systems, most likely due to the much longer range of the SMA potential.

Using only information for the bulk slab and for droplets containing at least 800 atoms, the Tolman length was obtained at the three temperatures of 1300, 1500, and 1700 K. Its variations with increasing gold concentration are depicted in Fig. 8. Note that the error bars are significant, as they result from the intrinsic error bars of the surface tension and from the dispersion around the linear fit. Despite such error bars, the Tolman length δ inferred from the variations of the surface tension with curvature lies within the rather well-defined range of 2–2.8 Å, close to the atomic radii. The Tolman length exhibits smooth variations with increasing gold concentration, which follow approximately linear relations. The slope of this relation increases with temperature, but in very modest amplitude (about 10%).

IV. CONCLUSIONS AND OUTLOOK

The surface tension is one of the primary properties causing order and segregation in metal alloys, however it is difficult to measure experimentally. Both features are especially true at the nanoscale where a large proportion of atoms lie at the surface, therefore it is highly desirable to develop theoretical approaches as a predictive alternative. In the present work, we have computationally studied the surface properties of silver-gold liquid alloys, in the limit of a bulk planar

slab and for various spherical droplets. Molecular dynamics simulations were carried out with an explicit many-body potential parametrized to reproduce low-temperature properties of the pure metals and the alloys, and the surface tension was obtained from the components of the pressure tensor normal and tangential to the liquid-vapor interface.

The potential was found to underestimate the measured surface tensions by a significant amount, however the experimental trend upon alloying was reproduced quite satisfactorily. In particular, the convex variations of the surface tension with increasing gold concentration are correctly captured by the simple perfect solution model, which treats the surface free energy from the weighted contribution of the pure metals.

Finite droplets containing between 100 and 3200 atoms have a significant curvature, which notably decreases the surface tension at all concentrations. In absence of direct experimental comparison with silver-gold nanoalloys, the present results confirm earlier results obtained for bulk alloys,[40] or for pure metals at the nanoscale,[21,22] at least qualitatively.

By providing convincing evidence that the surface tension of liquid silver-gold nanoalloys monotonically depends on size, composition, and temperature, we have also been able to determine the existence of a Tolman length and its positive sign. The value we estimate is comparable to the atomic radius, and minor but steadily increasing variations with gold concentration were found.

The present work could clearly be improved by devoting more efforts to the accurate parametrization of the many-body potential.[6] Unfortunately, methods using an explicit description of electronic structure will not be practical owing to the heavy statistical cost associated with converging the pressure tensor. Refining the potential by adding more terms, including *ab initio* data or finite temperature properties in the fitting process would all be useful in designing better model potentials for Ag-Au alloys.

The present investigation could also be extended to solid surfaces, rather than liquid-vapor interfaces. The computational methodology, which relied here on molecular dynamics, should then be replaced by the more convenient Monte Carlo framework, possibly enhanced with parallel tempering and preferential swapping.[32,42]

Finally, the dependencies of the surface tension on gold concentration could be incorporated in thermodynamical models aimed at building phase diagrams from a limited number of experimentally available data.[43] The Tolman length itself would be a valuable addition to such models in order to improve their predictive capabilities in the case of nanoscale alloys.

ACKNOWLEDGMENTS

The author wishes to acknowledge generous computational resources from the regional Pôle Scientifique de Modélisation Numérique in Lyon. Support is acknowledged from COST MP0903 Nanoalloy.

[1] I. Egry, E. Ricci, R. Novakovic, and S. Ozawa, Adv. Colloid Interface Sci. **159**, 198 (2010).
[2] J. A. V. Butler, Proc. R. Soc. London, Ser. A **135**, 348 (1932).
[3] M. S. Daw, and M. I. Baskes, Phys. Rev. B **29**, 6443 (1984).
[4] S. M. Thompson, K. E. Gubbins, J. P. R. B. Walton, R. A. R. Chantry, and J. S. Rowlinson, J. Chem. Phys. **81**, 530 (1984).
[5] B. Sadigh, and G. Grimwall, Phys. Rev. B **54**, 15742 (1996).
[6] E. B. Webb III and G. S. Grest, Phys. Rev. Lett. **86**, 2066 (2001).
[7] G. Grochola, S. P. Russo, I. Yarovsky, and I. K. Snook, J. Chem. Phys. **120**, 3425 (2004).
[8] H. Y. Hou, G. L. Chen, G. Chen, and Y. L. Shao, Comput. Mater. Sci. **46**, 516 (2009).
[9] B. Smit, A. G. Schlijper, L. A. M. Rupert, and N. M. van Os, J. Phys. Chem. **94**, 6933 (1990).
[10] W. Yu, and D. Stroud, Phys. Rev. B **56**, 12243 (1997).
[11] B. J. Block, S. K. Das, M. Oettel, P. Virnau, and K. Binder, J. Chem. Phys. **133**, 154702 (2010).
[12] A. E. van Giessen and E. M. Blokhuis, J. Chem. Phys. **131**, 164705 (2009).
[13] J. C. Tolman, J. Chem. Phys. **17**, 118 (1949).
[14] D. I. Zhukhovitskii, Russ. J. Phys. Chem. **75**, 1043 (2001).
[15] M. J. Haye and C. Bruin, J. Chem. Phys. **100**, 556 (1994).
[16] A. E. van Giessen and E. M. Blokhuis, J. Chem. Phys. **116**, 302 (2002).
[17] L. Granasý, J. Chem. Phys. **109**, 9660 (1998).
[18] K. Koga, X. C. Zeng, and A. K. Shchekin, J. Chem. Phys. **109**, 4063 (1998).
[19] M. P. Moody and P. Attard, Phys. Rev. Lett. **91**, 056104 (2003).
[20] V. G. Baidakov, G. Sh. Boltachev, and G. C. Chernykh, Phys. Rev. E **70**, 011603 (2004).
[21] M. Tanaka, T. Noda, O. Sakata, H. Terauchi, and I. Takahashi, in *Proceedings of the 8th Conference of the Asian Crystallographic Association (AsCA07)*, Taipei, 2007.
[22] S. Masada, and S. Sawada, Eur. Phys. J. D **61**, 637 (2011).
[23] T. B. Massalski, J. L. Murray, L. H. Bernett, and H. Baker, *Binary Alloy Phase Diagrams* (American Society for Metals, Metals Park, OH, 1986), Vol. 1.
[24] G. N. Derry, and R. Wan, Surf. Sci. **566–568**, 862 (2004).
[25] I. Srnová-Sloufová, B. Vickova, Z. Bastl, and T. L. Hasslett, Langmuir **20**, 3407 (2004).
[26] K. Kim, K. L. Kim, J.-Y. Choi, H. B. Lee, and K. S. Shin, J. Phys. Chem. C **114**, 3448 (2010).
[27] G. Bozzolo, J. E. Garcés, and G. N. Derry, Surf. Sci. **601**, 2038 (2007).
[28] G. Rossi, R. Ferrando, A. Rapallo, A. Fortunelli, B. C. Curley, L. D. Lloyd, and R. L. Johnston, J. Chem. Phys. **122**, 194309 (2005).
[29] F. P. Buff, J. Chem. Phys. **23**, 419 (1955).
[30] A. Rapallo, G. Rossi, R. Ferrando, A. Fortunelli, B. C. Curley, L. D. Lloyd, G. M. Tarbuck, and R. L. Johnston, J. Chem. Phys. **122**, 194308 (2005).
[31] F. Cleri, and V. Rosato, Phys. Rev. B **48**, 22 (1993).
[32] F. Calvo, E. Cottancin, and M. Broyer, Phys. Rev. B **77**, 121406(R) (2008).
[33] F. Calvo, J. Phys. Chem. C **115**, 17730 (2011); *ibid.* **116**, 7607 (2012).
[34] B. D. Todd and R. M. Lynden-Bell, Surf. Sci. **281**, 191 (1993).
[35] J. H. Irving and J. G. Kirkwood, J. Chem. Phys. **18**, 817 (1950).
[36] B. Hafskjold and T. Ikeshoji, Phys. Rev. E **66**, 011203 (2002); T. Nakamura, W. Shinoda, and T. Ikeshoji, J. Chem. Phys. **135**, 094106 (2011).
[37] R. A. van Santen and M. A. M. Boersma, J. Catal. **34**, 13 (1974).
[38] R. Bouwman, L. H. Toneman, M. A. M. Boersma, and R. A. van Santen, Surf. Sci. **59**, 72 (1976).
[39] R. C. Weast, *Handbook of Chemistry and Physics*, 61st ed. (CRC, Boca Raton, FL, 1980).
[40] G. Bernard, and C. H. P. Lupis, Metall. Trans. **2**, 555 (1971).
[41] J. G. Powles, R. F. Fowler, and W. A. B. Evans, Phys. Lett. A **98**, 421 (1983).
[42] F. Calvo, Faraday Discuss. **138**, 75 (2008).
[43] H. L. Lukas, S. G. Fries, and B. Sundman, *Computational Thermodynamics, The Calphad Method* (Cambridge University Press, Cambridge, 2007).